Available online at www.sciencedirect.com
ScienceDirect
C. R. Physique 8 (2007) 385–395
COMPTES RENDUS PHYSIQUE
http://france.elsevier.com/direct/COMREN/

Optical techniques for direct imaging of exoplanets/Techniques optiques pour l'imagerie directe des exoplanètes

The Achromatic Interfero Coronagraph

Yves Rabbia [a,*], Jean Gay [a], Jean-Pierre Rivet [b]

[a] *Observatoire de la Côte d'Azur, Département Gemini, UMR CNRS 6203, Av. Copernic, 06130 Grasse, France*
[b] *Laboratoire Cassiopee, CNRS, Observatoire de la Côte d'Azur, BP 4229, F-06304 Nice cedex 04, France*

Available online 8 June 2007

Abstract

We report on the Achromatic Interfero Coronagraph, a focal imaging device which aims at rejecting the energy contribution of a point-like source set on-axis, so as to make detectable its angularly-close environment (applicable to stellar environment: circumstellar matter, faint companions, planetary systems, but also conceivably to Active Galactic Nucleii and multiple asteroïds).

With AIC, starlight rejection is based on destructive interference, which allows exploration of the star's neighbourhood at an angular resolution better than the diffraction limit of the hosting telescope. Thanks to the focus crossing property of light, rejection is achromatic thus yielding a large spectral bandwidth of work. Descriptions and comments are given regarding the principle, the device itself, the constraints and limitations, and the theoretical performance. Results are presented which demonstrate the close-sensing capability and which show images of a companion obtained in laboratory and 'on the sky' as well. A short pictorial description of the alternative AIC concepts, CIAXE and Open-Air CIAXE, currently under study, is given. ***To cite this article: Y. Rabbia et al., C. R. Physique 8 (2007).***

Résumé

Le Coronographe Interférentiel Achromatique. On présente le Coronographe Interférentiel Achromatique (AIC dans le texte), un système imageur en mode coronographique pour rejeter de l'image, la contribution d'une source ponctuelle sur l'axe de visée afin de laisser apparaître son environnement angulairement proche (cela concerne les étoiles : matière circumstellaire, compagnons faibles, systèmes exoplanétaires, mais potentiellement aussi les Galaxies à noyau actif et les astéroïdes multiples).

Avec le AIC, la réjection sur l'axe procède par interférences destructives, ce qui permet une exploration du voisinage stellaire dans une proximité angulaire meilleure que celle fixée par la limite de diffraction du télescope. Le principe de la réjection utilise le passage d'une onde par un foyer ce qui la rend achromatique et permet ainsi d'observer à large bande spectrale. On décrit le principe et l'architecture du coronographe, les contraintes instrumentales, les limitations associées, et les performances théoriques en réjection. Des résultats de tests, en laboratoire et en observation sur le ciel, sont donnés, en terme d'images montrant les capacités de sondage proche et de détection d'un compagnon faible. Une brève présentation graphique de deux concepts CIAXE et Open-Air CIAXE (actuellement en phase d'étude) dérivés du principe générique est donnée. ***Pour citer cet article : Y. Rabbia et al., C. R. Physique 8 (2007).***

Keywords: Stellar coronagraphy; High contrast imaging; Nulling techniques

Mots-clés : Coronographie stellaire ; Imagerie à haut contraste ; Interférométrie annulante

* Corresponding author.
E-mail addresses: yves.rabbia@obs-azur.fr (Y. Rabbia), jean.gay@obs-azur.fr (J. Gay), jean-pierre.rivet@obs-nice.fr (J.-P. Rivet).

1631-0705/$ – see front matter
doi:10.1016/j.crhy.2007.04.003

1. Introduction

The Achromatic Interfero Coronagraph (AIC in the following) is a focal imaging device working in coronagraphic mode and meant as a tool for the study of stellar environment (Gay and Rabbia [1], Gay et al. [2], Baudoz et al. [3,4]). The purpose of stellar coronagraphy is to make detectable images of the faint emitting features located angularly very close to an unresolved source whose brightness is tremendously larger (typically 10^4 to 10^6 times larger) than any of the surrounding features. This is the case for stars, but also for other celestial sources, such as for example Active Galactic Nucleii and asteroids with multiple components. In the following we use 'star' and 'companion' to denote respectively the central source and any neighbouring feature. Any coronagraph aims at lowering as far as possible the energy contribution of the parent star in the recorded image, which would otherwise prevent the detection of the companion. The goal is thus to perform the 'extinction' of the star while keeping the off-axis components transmitted as completely as possible to the detector in the image plane. This extinction capability, is usually expressed by the 'Rejection rate' defined by $Rej = F_{\text{collected}}/F_{\text{residual}}$, where F_{residual} and $F_{\text{collected}}$ are the fluxes recorded with and without coronagraphic effect, respectively.

Not only the rejection capability is required but also the 'close-sensing' capability: rejection must apply only within a very small angular extension, called the Inner Working Angle (IWA in the following) around the pointing direction, otherwise companions are also rejected.

In addition, the rejection ought to apply over as large as possible a spectral bandwidth, benefiting to the detection capabilities in several respects: increase of Signal to Noise Ratio (SNR), adaptability to the science target by flexible choice of dedicated spectral intervals, enhancement of detectivity by a differential data processing, the 'adapted scale image subtraction' (Gay et al. [5], Rabbia et al. [6]) inspired by a method introduced by (Racine et al. [7]).

Early stellar coronagraphs have been a transposition to stars of the scheme initially introduced by B. Lyot (Lyot [8]) to study the solar corona. The technique relies on a tiny opaque mask set at the focus of an intermediate image plane, so as to block photons from the on-axis source, while photons from the companion are transmitted to the ultimate image plane. Because of diffraction effects the mask must cover several Airy radii (λ/D): working wavelength/(diameter of the telescope) what makes the 'close-sensing capability' comparatively poor (Mouillet et al. [9], Beuzit et al. [10]).

Another approach, called interfero-coronagraphy, yields the extinction from a destructive interference process. The collected incident wave is split into two components, which are recombined after insertion of a π phase shift between them. Thus the recombination (coherent addition of fields at the detector) results in destructive interference and ideally no photon from the on-axis source can reach the detector. Here, thanks to the coherence properties of light, an angular sensing capability at a level better than the diffraction limit (λ/D), is achievable. The subsequent counterpart is a limitation of extinction (finite star size and random tilt of incident wavefront).

As early as 1996, the concept of the AIC has been suggested (Gay and Rabbia [1], Gay et al. [2]) from which various prototypes have been developed and used for tests in the laboratory (Baudoz [3], Rivet et al. [11]) and 'on the sky' (Baudoz et al. [4,12]) on ground-based telescopes (although AIC has been initially devised for space-based operation (Rabbia et al. [13])). Besides, even although coronagraphs are generally meant as working with a single compact aperture, AIC can be used for nulling interferometry (Gay and Rabbia [1], Rabbia et al. [14]), for example, in a two-aperture Bracewell configuration (Bracewell [15]). The immediate and essential requirement to obtain the coronagraphic effect with AIC is that the (complex) transmission of the aperture must be centro-symmetric (insensitive to a 180 degrees rotation).

Other concepts for interfero-coronagraphy, each using a specific type of beam separation/recombination have been devised since. Let us cite among other early concepts: the Phase Mask Coronagraph – PMC – (Roddier and Roddier [16]), the Sectorized Phase Mask Coronagraph – SPMC – (Rouan et al. [17]), and the Phase Knife Coronagraph – PKC – (Abe et al. [18]).

The main specific feature and advantage of AIC is the achromaticity of the phase shift process, which was not the case for the others cited, early interfero-coronagraph designs, and for the Lyot configuration as well. Another one concerns the IWA, with the best close-sensing capability (Guyon et al. [19]). Another specific feature is that AIC yields two twin-images of the companion (displayed symmetrically with respect to the pointing axis), each conveying $1/4$ of the collected energy. This can be seen as a drawback because of a reduced transmission and because of the symmetrisation of companions (point-like or extended). Actually this is an advantage for point-like companions whose separations and orbits can be better determined from the twin-images.

In this article we give but a kind of status report on the AIC (a comparison between AIC and other coronagraphs is given in (Guyon et al. [19])) focusing, for the reader's convenience, on the underlying algebraic formalism, although recalling only basic lines because of space limitation. In Section 2 we describe the principle of the device and the device itself and we give a short pictorial description of alternative AIC devices, currently under study (Gay et al. [20, 21]). In Section 3 we describe the constraints for both implementation and operation, and we outline the theoretically expected capabilities of AIC. In Section 4 we give results from testing AIC both in the laboratory and 'on the sky'.

2. Basic principle

2.1. Functional description and pictorial summary

Basically, the AIC is a Michelson–Fourier interferometer modified by inserting on one arm an achromatic π phase shift and a pupil rotation by 180 degrees. This double operation is performed by a cat's eye optical system, where the π phase shift originates in the focus crossing property (Gouy [22], Born and Wolf [23], Boyd [24]). The collimated beam from the telescope is split in two sub-beams, forming the two interferometric arms, one (the 'fc' arm), where the focus-crossing occurs, the other (the 'ff' arm) which includes a train of flat mirrors to balance the optical paths in the interferometer. In the design these optical paths are equal, but some spurious residual Optical Path Difference (OPD) might still occur at the implementation and must be controlled. The beamsplitter at entry is used also for the recombination of beams. As a pictorial summary, Fig. 1 illustrates these comments.

Mono-axial configurations, easier to insert in a telescope's optical train (Gay et al. [20,21]) have been devised, and are currently under study: the CIAXE and the open-air CIAXE. Fig. 2 systematically illustrates the paths of beams for these two concepts, and shows how the generic functions (beamsplitting, focus-crossing, recombination, zero-OPD) are performed.

2.2. Physical description

The typical AIC device (Fig. 3) consists of a kit of optical components assembled on a basement comprising two galleries for beams to travel in air. All elements are in silica and assembling is made using molecular bonding under interferometric control. Optical paths are equalized by construction; however, a fine-tuning of OPD (few nanometers) remains possible. The K photometric window ($\lambda = 2.2$ µm, $\Delta\lambda = 0.4$ µm being a convenient spectral interval (regarding both science and constraints), the beamsplitter cube is optimized for $\lambda = 2.2$ µm but it can work with a bandwidth larger than the K-band. The remaining components, being mirrors, are achromatic by nature.

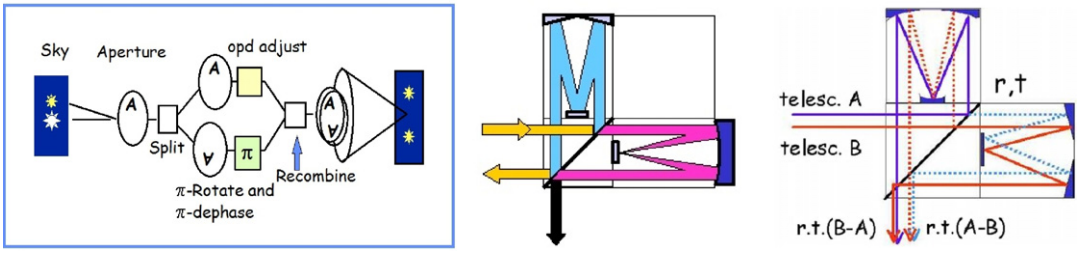

Fig. 1. Schematic illustration of AIC functions (left) the configuration of beams in single aperture mode (center) the routing of beams with a two-aperture interferometer (right).

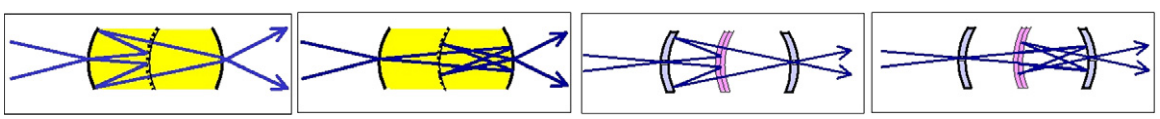

Fig. 2. Schematic description with separated beam routes for CIAXE (left) and for Open-Air CIAXE (right), where generic functions of AIC appear. In CIAXE beam entry and exit are small uncoated area, while they are holes in Open-Air CIAXE. Typical overall volume roughly is the one of a cylinder 4 cm×3 cm length×diameter.

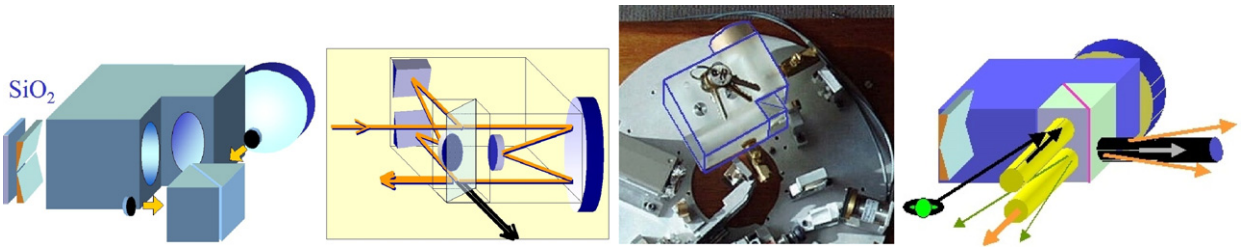

Fig. 3. From left to right: the kit of elements, the life of an on-axis beam and the two exit ports, AIC itself in an optical interface for accommodation on a telescope, the making of the output beams from both on-axis and off-axis sources.

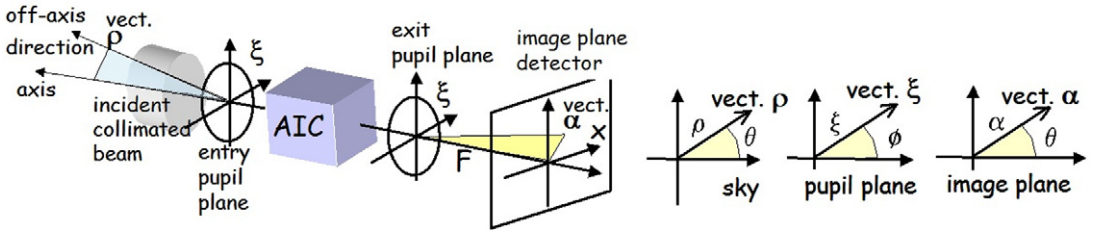

Fig. 4. Schematic description of the notation used.

An incident collimated on-axis beam yields two perpendicular output beams. One, the constructive port, conveys all collected energy while no photon goes into the other, the destructive port. An off-axis source yields two symmetrically oriented sub-beams at each exit port. Each exiting sub-beam conveys 1/4 of the energy collected from the companion.

2.3. *Formalism and algebraic description of the principle*

The formalism is the one of Fourier optics (Goodman [25]), involving a pupil plane and an image plane. The cat's eye being designed for this purpose, the two arms share the same pupil plane, placed at the exit collimator, which focuses the recombined beams to the detector set in the image plane.

Coordinates are vectorial even although we frequently denote them by a single letter. We use their reduced form (dimensionless). Thus, a coordinate in the pupil plane is denoted ξ and means (vector in pupil plane)/(wavelength), whereas α is an angular measurement (radians) and means (vector in image plane)/(focal length of exit collimator). The magnification factor between entry and output pupil planes is set as unity; thus α is associated to an angle over the sky, frequently denoted ρ (a vector). All vector coordinates are sometimes expressed using polar coordinates (ξ, ϕ) and (α, θ) or (ρ, θ) where ξ, ρ and α are then the moduli, whilst ϕ and θ are the polar angles. Fig. 4 illustrates the notations used. Complex amplitudes of fields are noted $\psi_{\text{collected}}$ and ψ_{recomb} at the entry and at the exit pupil planes, respectively. The transmission $P(\xi)$ at the aperture is complex. Reflection and transmission coefficients for complex amplitude at the beamsplitter are respectively noted r and t, with, as usual, $R = |r|^2$ and $T = |t|^2$. Ideally $R = T = 0.5$.

2.3.1. *Destructive interference process and off-axis images*

The complex amplitude of the field entering the AIC is $\psi_{\text{collected}}(\xi) = A.P(\xi).e^{i.\varphi(\xi)}$ since some phase distortions $\varphi(\xi)$ might exist in the collected wavefront. The field amplitude A is such that $|A|^2 = \Omega$, the brightness of the on-axis source. At recombination, each sub-field have been both transmitted and reflected at the beamsplitter. On its way each field might experience phase distortions (optical defects) and conveys the phase variation caused by propagation along the arm. In addition an extra optical path (yielding φ_{opd}) can be inserted and eventually fine-tuned in the 'ff' arm. Moreover, in the 'fc' arm the π phase shift occurs and $\psi_{\text{collected}}(\xi)$ is symmetrized by the 180 degrees rotation of pupil, thus yielding $\psi_{\text{collected}}(-\xi)$. At recombination we have $\psi_{\text{recomb}}(\xi) = \psi_{\text{ff}}(\xi) + \psi_{\text{fc}}(\xi)$ whose explicit expression depends on the exit port. At the destructive port we have:

$$\psi_{\text{ff}}(\xi) = r.t.A.P(\xi).\left[e^{i.\varphi(\xi)}.e^{i.\varphi_{\text{ff}}(\xi)}.e^{i.\varphi_{\text{ff\_path}}}.e^{i.\varphi_{\text{opd}}}\right]$$

and

$$\psi_{\mathrm{fc}}(\xi) = r.t.A.P(-\xi).\left[\mathrm{e}^{\mathrm{i}.\pi}.\mathrm{e}^{\mathrm{i}.\varphi(-\xi)}.\mathrm{e}^{\mathrm{i}.\varphi_{\mathrm{fc}}(\xi)}.\mathrm{e}^{\mathrm{i}.\varphi_{\mathrm{fc\_path}}}\right]$$

At the constructive port, $\psi_{\mathrm{ff}}(\xi)$ keeps the same expression, while the π phase shift factor $\mathrm{e}^{\mathrm{i}.\pi}$ is replaced by unity in $\psi_{\mathrm{fc}}(\xi)$. In these description φ_{ff} and φ_{fc} are gathering internal phase defects in the respective arms. All phase terms are chromatic, but for easier reading, λ is omitted in the formulae.

In an ideal situation, all mentioned phases are zero and optical paths are equal, hence we have:

$$\psi_{\mathrm{recomb}}(\xi) = r.t.A.\left[P(\xi) - P(-\xi)\right]$$

Thus, as soon as the complex transmission is centro-symmetric ($P(\xi) = P(-\xi)$) we find that $\psi_{\mathrm{recomb}}(\xi)$ is uniformly zero. Hence photons from the on-axis source do not reach the detector's plane (they are sent back to the sky via the constructive port). This complete cleaning of the image plane for stellar photons in the ideal case is specific to AIC. Therefore, there is no geometrical link between the rejection lobe (IWA) and the energy distribution in the image plane.

For a companion, off-axis by ρ, we have

$$\psi_{\mathrm{collected}}(\xi) = A.P(\xi).\mathrm{e}^{-\mathrm{i}.2.\pi.\xi.\rho}$$

and at recombination we find

$$\psi_{\mathrm{recomb}}(\xi) = r.t.A.P(\xi)\left[\mathrm{e}^{-\mathrm{i}.2.\pi.\xi.\rho} - \mathrm{e}^{+\mathrm{i}.2.\pi.\xi.\rho}\right]$$

which is not zero, so that some light escapes the destructive process (let us note that, without the pupil rotation, we would find zero just like the case of the on-axis source). Moreover, the system yields two twin-images of the companion, as described below, using Fourier optics. The intensity in image plane is

$$I(\alpha, \rho) = \left|\widehat{\psi}_{\mathrm{recomb}}(\alpha)\right|^2$$

Since we have

$$\widehat{\psi}_{\mathrm{recomb}}(\alpha) = r.t.\widehat{P}(\alpha) * \left[\delta(\alpha - \rho) - \delta(\alpha + \rho)\right]$$

we end up (usual complex notations) with

$$I(\alpha, \rho) = R.T.\Omega.\left[\left|\widehat{P}(\alpha - \rho)\right|^2 + \left|\widehat{P}(\alpha + \rho)\right|^2 - 2.Re\left(\widehat{P}(\alpha - \rho).\widehat{P}^*(\alpha + \rho)\right)\right]$$

that shows the presence of twin images (centro-symmetrically located Airy patterns) and of a cross-term. This latter term vanishes as ρ increases (enlarged separation, product of amplitudes null). Conversely, it makes the intensity progressively cancel as ρ goes to zero (companion no longer off-axis, hence undergoing rejection). We report in Fig. 5 a pictorial summary of the destructive interference process both for star and companion, in terms of both wavefronts and complex amplitudes.

When departing from the ideal situation, all phases just mentioned are no longer zero, but we still assume $P(\xi) = P(-\xi)$, the essential requirement for the coronagraph to work properly. The amplitude at recombination now is (with self-explanatory notations):

$$\psi_{\mathrm{recomb}}(\xi) = r.t.A.P(\xi)\left[\mathrm{e}^{\mathrm{i}.\varphi_1(\xi)} - \mathrm{e}^{\mathrm{i}.\varphi_2(\xi)}\right]$$

which is clearly not zero, so that a residual energy is found in the image plane and rejection has a finite value, whose expression we now derive.

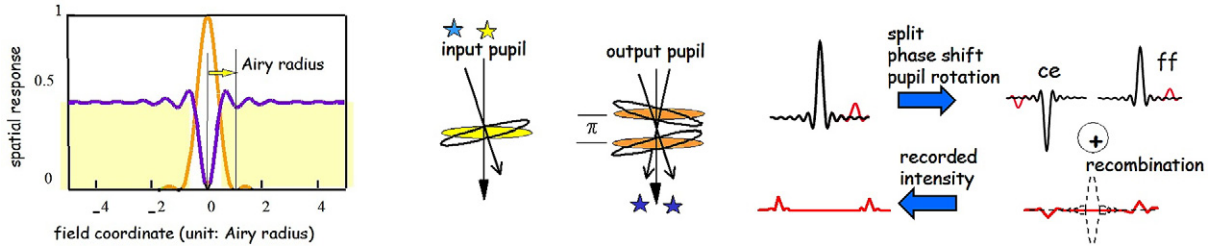

Fig. 5. Left: the radial profile of the spatial response of AIC (circular symmetry); center and right: pictorial description of the destructive interference process, wavefront behaviour, and amplitude behaviour.

2.3.2. Expression of the rejection from integrated energy in image plane

In the introduction, rejection has been defined by the ratio $Rej = w_0/w$ with w and w_0 the intensities recorded respectively with and without the coronagraphic effect (in other words at destructive and constructive ports). With this definition we have in real situation

$$Rej = \frac{w_0}{w} = \frac{\int |P(\xi).\mathrm{e}^{\mathrm{i}.\varphi_1(\xi)} + P(-\xi).\mathrm{e}^{\mathrm{i}.\varphi_2(\xi)}|^2\,\mathrm{d}\xi}{\int |P(\xi).\mathrm{e}^{\mathrm{i}.\varphi_1(\xi)} - P(-\xi).\mathrm{e}^{\mathrm{i}.\varphi_2(\xi)}|^2\,\mathrm{d}\xi}$$

The phase factor that might occur in $P(\xi)$ is reported in the incident wavefront phase distortions, so that $P(\xi)$ is real and, in addition, we assume

$$P(\xi) = \Pi\left(\frac{\xi}{D}\right) = \left|P(\xi)\right|^2$$

the usual 'Camembert-like' transmission (1 inside, 0 outside the disk of diameter D). Moreover, it is reasonable to assume that the various phase terms are small, so that using the approximation $\mathrm{e}^{\mathrm{i}.x} = 1 + \mathrm{i}.x + \cdots$ we can write:

$$Rej = \frac{\int_{\text{pupil}}(1 + \cos\Delta\varphi(\xi)).\mathrm{d}\xi}{\int_{\text{pupil}}(1 - \cos\Delta\varphi(\xi)).\mathrm{d}\xi} \approx \frac{4}{\int_{\text{pupil}} |\Delta\varphi(\xi)|^2\,\mathrm{d}\xi} = \frac{4}{\sigma^2_{\Delta\varphi}}$$

where we have introduced the differential phase $\Delta\varphi(\xi)$ such that:

$$\Delta\varphi(\xi) = \left[\varphi(\xi) - \varphi(-\xi)\right] + \left[\varphi_{\text{ff}}(\xi) - \varphi_{\text{fc}}(\xi)\right] + \left[\varphi_{\text{ff\_path}} - \varphi_{\text{fc\_path}} + \varphi_{\text{opd}}\right]$$

and where φ_{opd} allows one to adjust the mean-value to zero, hence the use of the variance $\sigma^2_{\Delta\varphi}$. The respective expressions of integrated energy at constructive and destructive ports are $w_0 = 4.R.T.\Omega.S$ and $w = [w_0/4].\sigma^2_{\Delta\varphi}$, where S is the area of the collecting aperture.

From the generic expression $Rej = 4/\sigma^2_{\Delta\varphi}$, the rejection can be evaluated in connection with the various phase defects and conversely, technical specifications (tolerancing) can be defined according to a targeted rejection; this is considered later in the text.

Let us note that, although this definition is a general and widespread convention, it rather traces the quality of the set-up than the ability to detect a companion, since it does not consider the shape of the energy distribution in the image plane. Therefore, for a companion imaged at a location free from residual energy, this integrated quantity is not appropriate and likely to be pessimistic. This point is also discussed later in the text.

2.3.3. Spatial response of AIC: close-sensing

To evaluate the close-sensing capability (in other words, beyond which angular separation can the companion be seen?) we consider a point-like source off-axis by ρ, and we integrate the energy in the image plane to obtain the recordable energy with respect to ρ, what describes the spatial response $w(\rho)$ of the AIC ($w(\rho)$ has a circular symmetry).

With our notations the brightness distribution (using the Dirac δ symbol) is $\Omega(\alpha, \rho) = \Omega.\delta(\alpha - \rho)$. Here we momentarily drop all spurious phase effects, including OPD misbalance; hence $\Delta\varphi(\xi) = 0$. We have then

$$\psi_{\text{collected}} = A.P(\xi).\mathrm{e}^{-\mathrm{i}.2\pi.\xi.\rho}$$

and using the Parseval–Plancherel theorem we can write:

$$w(\rho) = \int I(\alpha, \rho).\mathrm{d}\alpha = \int \left|\widehat{\psi}_{\text{recomb}}(\alpha, \rho)\right|^2.\mathrm{d}\alpha = \int \left|\psi_{\text{recomb}}(\xi, \rho)\right|^2.\mathrm{d}\xi$$

More explicitly, using polar coordinates (ξ,ϕ) in pupil plane and (ρ, θ) for the off-axis direction, we write:

$$w(\rho) = 2.R.T.\Omega.\int_0^{2.\pi}\int_0^{D/2}\left(1 - \mathrm{e}^{-\mathrm{i}.2.\pi.(2.\xi.\rho).\cos(\phi-\theta)}\right).\xi.\mathrm{d}\xi.\mathrm{d}\phi$$

Thus, from Hankel's transform properties (Bracewell [26]) we end up with the spatial transmission or rejection lobe (circular symmetry, sky coordinate ρ):

$$w(\rho) = 2.R.T.\Omega.\left(\frac{\pi.D^2}{4}\right).\left[1 - \frac{2.J_1(2.\pi.D.\rho)}{2.\pi.D.\rho}\right]$$

where the Airy distribution (for amplitudes) appears, associated to a telescope of diameter $2D$. Fig. 5 illustrates the radial profile of the function $w(\rho)$, showing the close-sensing capability of AIC and how it beats the diffraction-limit. Namely, the maximal transmission occurs at less than the telescope's first Airy (λ/D) ring. For an off-axis source at $\rho = 0.3$ Airy, the transmission remains 0.5 of that far from axis (Baudoz [3]).

3. Operational and technical constraints, associated limitations and theoretical capabilities

For the coronagraphic effect to work, two immediate constraints apply: (i) the complex transmission at exit pupil plane must be insensitive to a 180 degrees rotation, and (ii) the optical path difference (opd) must accurately be zero. Other constraints concern the technical specifications and the conditions of observation.

Regarding the symmetry of the pupil, problems might arise from the amplitude of the transmission $P(\xi)$, because of the central obscuration and the spider bearing it (central-symmetry would possibly be broken). Then, by inserting a suitably designed mask in an auxiliary pupil plane, centro-symmetry is recovered; thus this constraint is not a heavy one. We report in Fig. 6 an illustration of both the trouble and the remedies. Problems regarding the phase of the complex transmission are by far more serious and are considered later in the text.

Residual Optical Path Difference (OPD) and optical defects. OPD between interfering waves works as a weight applied to the contribution of the on-axis source. As the OPD goes away from zero, the on-axis source gradually appears in the image, and this rapidly degrades the rejection. This is schematically illustrated in Fig. 6. Either for a residual OPD or for optical defects we use the formula $Rej = 4/\sigma^2_{\Delta\varphi}$ but in place of $\sigma^2_{\Delta\varphi}$, which makes sense only for optical defects, we directly take $[4.\pi^2/\lambda^2].\delta^2$ where δ stands for either the residual OPD or for the standard-deviation of surface defects over the pupil. Then, with a target rejection G we define the tolerance on δ via $Rej \geqslant G$ which yields the condition $\delta \leqslant \lambda/(\pi.\sqrt{G})$. For example, with $G = 10^4$ the constraint on δ is roughly $\lambda/300$ and for $G = 10^5$ it is $\lambda/1000$, which are rather stringent constraints so that interferometric control is mandatory when assembling the AIC. The same range of specifications applies, for example, to the beamsplitting cube, where internal reflected waves must be kept destructively interfering; this is a matter of well-controlled optical paths within the cube. Moreover, phase defects occurring inside the AIC cannot be corrected for, and degrade the rejection.

3.1. Limitations from conditions of observation

Basically, stellar leakage and wavefront phase distortions are the immediate causes limiting the rejection. Stellar leakage occurs with any nulling technique, when the star has a finite angular diameter and is incompletely eliminated by the spatial response because its profile around origin is not flat. Wavefront distortions originate in deterministic optical defects (arising in the optical train) and random distortions induced by atmospheric turbulence, this latter causing the major limitation in ground-based observations (with tip/tilt fluctuations being the heaviest contributor). Another constraint occurs because of atmospheric refraction (beyond the scope of this article). With space-based observations, beside fine guidance residual fluctuations (jitter) only faint internal phase defects are occurring and are not that big a concern (Baudoz [3], Rabbia et al. [13]).

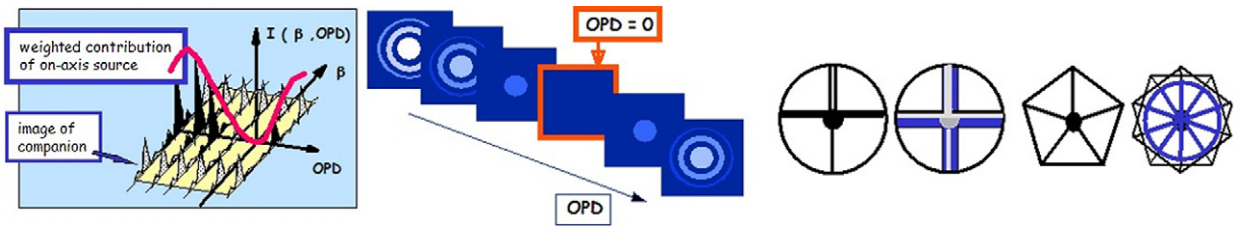

Fig. 6. Left and center: pictorial illustration of the role of OPD; right: recovering amplitude centro-symmetry in the collecting aperture, by using appropriate masks in intermediate pupil plane.

Stellar leakage, denoted $w(\Theta)$ for a star whose brightness distribution is $\Omega(\rho) = \Omega.\Pi(\frac{\rho}{\Theta})$ with angular diameter Θ, is evaluated by the integral of the spatial response $w(\rho)$ taken over the brightness distribution. Again from Hankel's transform properties we have:

$$w(\Theta) = \int_0^{2.\pi} \int_0^{\Theta/2} w(\rho).\rho.\mathrm{d}\rho.\mathrm{d}\theta = 2.R.T.\Omega.\left[1 - \frac{J_0(\pi.D.\Theta)}{(\pi.D.\Theta)^2/4}\right]$$

As an example for $\Theta = 0.05$ Airy radius, stellar leakage (residual/collected) is 0.001 (Baudoz et al. [4]).

Random phase distortions from atmospheric turbulence. The spurious phase distribution is denoted:

$$\Delta\varphi(\rho,\theta) = \varphi(\rho,\theta) - \varphi(\rho,\theta+\pi)$$

usually expressed as an infinite weighted sum of Zernike orthogonal polynomials

$$\varphi(\rho,\theta) = \sum_{j=1}^{\infty} w_j.Z_j(\rho,\theta)$$

where the w_j are random and trace the effect of turbulence. The resulting variance $\sigma^2_{\Delta\varphi}$ must be reduced by using an Adaptive Optics (AO) system. Its role is to induce appropriate phase distortions so as to absorb some of the incident ones. Note that centro-symmetric phase distortions automatically cancel, whilst other are amplified; however, a significant gain remains by using AO (Baudoz et al. [4]). For convenience, we refer to the Zernike formalism (Noll [27]) to theoretically describe the action of AO, which leads to a corrected phase distribution

$$\varphi_{\mathrm{corr}}(\rho,\theta) = \varphi(\rho,\theta) - \sum_{j=1}^{J} a_j.Z_j(\rho,\theta)$$

where J is the highest Zernike order included in the correction. The resulting variance is significantly less than the previous one, and hence there is a better rejection. The result in the image is a centro-symmetric speckle pattern, whose time-averaged distribution looks like a halo (volcano + caldera-shaped). Algebraic derivation (Baudoz et al. [4]) shows that the higher the J, the larger the caldera (central dark hole) and the lower the edges of the volcano. Actually, this theoretical approach pertains to ultimate performance. Practically, since AO may work in various regimes (zonal, modal, Fourier basis set) the pure Zernike formalism might depart from real situations and expected corrections are not completely efficient (what we call 'incomplete correction') and estimations must be reviewed, using an example of actual AO performance (Conan [28]). Both estimates from numerical simulation are shown in Fig. 9.

Effect of residual tip/tilt phase defects. Incomplete tip/tilt correction (pointing jitter) causes the heaviest degradation and deserves a specific derivation. Taking into account that tip/tilt residuals are small, and using the approximation $2.J_1(z)/z \cong 1 - z^2/8$ the resulting average rejection is obtained from the averaged spatial response yielding:

$$\langle Rej\rangle = \frac{w_0}{\langle w(\rho)\rangle} \cong \frac{16}{(2.\pi.D/\lambda)^2.\langle\rho^2\rangle}$$

whence is extracted the constraint:

$$\sigma_\rho \leqslant \frac{airy}{\sqrt{\langle Rej\rangle}}$$

where $\langle Rej\rangle$ is the target rejection and $airy = 1.22\frac{\lambda}{D}$. For example, a 10^4 target leads to $\sigma_\rho \leqslant \frac{airy}{100}$. With HST ($D =$ 2.4 m) at 2.2 μm we find $\sigma_\rho \leqslant 10^{-8}$ rad or 0.002 arcsec, which is in the range of the HST fine guidance capability.

3.2. Theoretically expectable performance

Enhancement of detection capability by the 'scaled-subtraction' process. Thanks to the large spectral bandwidth allowed by AIC, two adjacent channels splitting the K window might be accommodated on the same detector. The respective residual speckles have homothetic patterns (scaling factor: λ). Therefore, in principle (thanks to the central 'dark-hole') it is possible to give them the same spatial distribution by properly scaling both the spatial extension and the intensity distribution. Then, images of a companion become shifted in one channel with respect to the other and

have unequal heights. Subtracting the re-scaled patterns tends to eliminate the speckles while a trace of the companion remains. This process (schematically summarized in Fig. 7), is described with numerical simulations in Gay et al. [5] and Verinaud and Carbillet [29]. In the case of an on-axis residual spurious contribution, the efficiency is reduced, but a significant gain in detection capability remains.

Signal to noise ratio for the detection of a companion. As already mentioned, using the integrated rejection $Rej = 4/\sigma^2_{\Delta\varphi}$ is not appropriate to evaluate the detection capability for a companion, the point being not to count unwanted photons in the whole image plane, but rather to distinguish the companion against the noisy and non-uniform residual energy distribution. Thus the convenient approach for theoretical assessments is to express a pixel-dependent Signal to Noise Ratio (SNR), taking into account the spatial response of the AIC, the intensity fluctuations (speckled halo) and the area covered by the companion's image (distance to axis and image extension). From a detailed analysis (Baudoz et al. [4]) the expression of this SNR (M recorded exposures, companion off-axis by angular vector ρ) is:

$$\mathrm{SNR}(\rho) = \frac{(N_c/4).\sqrt{2}.\sqrt{M}.\int_{\text{companion}} w(\alpha).C(\alpha-\rho).\mathrm{d}\alpha}{\sqrt{\int_{\text{companion}}[\mathrm{var}_{\text{residual}}(\alpha) + \mathrm{var}_{\text{bg}} + var_{\text{detect}}].\mathrm{d}\alpha}}$$

where the factor $(1/4)$ traces the transmission for a single image, $\sqrt{2}$ accounts for the two twin-images, $w(\rho)$ is the spatial response of AIC, and $C(\alpha-\rho)$ is the normalized distribution weighting of the companion's contribution (Airy-like shaped). Integration is taken over the pixels covered by the companion's image.

The number of collected photons from a m-magnitude star is

$$N_0 = \left[F_{\text{ref}}(\lambda)/h.\nu\right].10^{-0.4\ m}.[\eta.4.R.T.S.t_{\text{opt}}.\Delta\lambda.\tau]$$

with usual notations, while for the companion (magnitude difference Δm) we have

$$N_c = N_0.10^{-0.4\ \Delta m}$$

In the noise factor, variances are related to a given pixel: $\mathrm{var}_{\text{det}}$ is the readout noise variance (ron^2) of the detector, var_{bg} is for the background radiation (using Planck's formulae) and $\mathrm{var}_{\text{residual}}$ comes from the fluctuations of the residual energy distribution. This latter includes $g_J.N_0$, the residual energy when AO-corrections are carried up to the Zernike radial order J (each comprising several azimuthal orders), and is evaluated by the doubly stochastic process involving the Poisson photon noise at a given illumination level and the fluctuations of this level. Performance of the AIC (expressed as detectable Δm), directly depends on AO capabilities (Fig. 8).

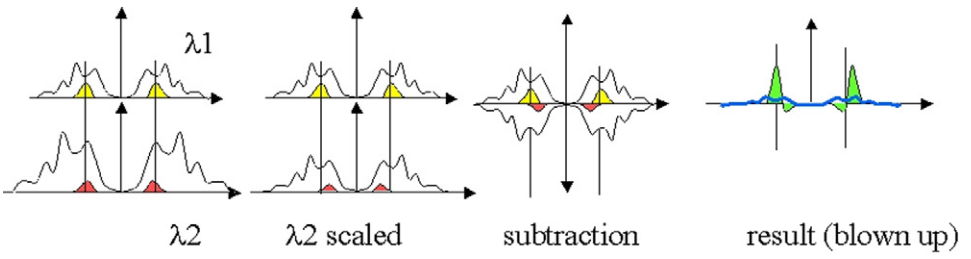

Fig. 7. Pictorial summary of the scaled-subtraction process.

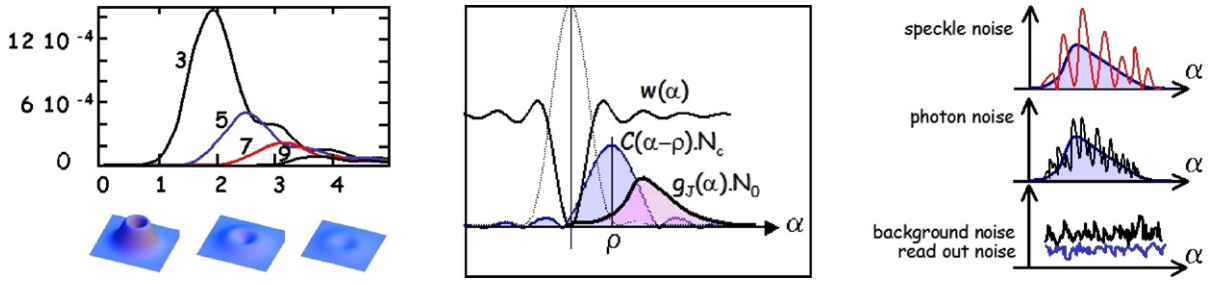

Fig. 8. Left: residual energy profiles with AO corrections up to 9 Zernike radial orders (meaning $J = 36$); center: notations for the SNR expression (only one-sided cuts featured); right: phenomenology of noise in the residual energy.

Illustrations for 'complete' and 'incomplete' corrections are given in Fig. 9, as well as the expected detection capabilities in space-based observation.

4. Results

The results obtained so far both in the laboratory and 'on the sky' are but illustrations of potential capabilities. To spare space we rely on a pictorial presentation, see Fig. 10 and Baudoz et al. [4,12] for details.

Close-sensing capability is clearly validated. The effective capability for the detection shows good agreement between expected and observed capabilities, taking into account the turbulence conditions and the AO performance.

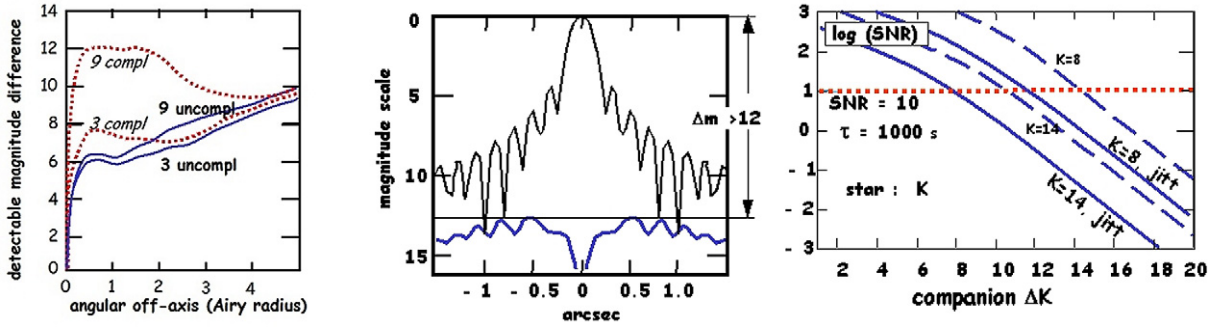

Fig. 9. Left: theoretically detectable magnitude difference of a companion versus its off-axis angle, showing both complete (ideal) and incomplete (real) AO corrections, for radial orders 3 and 9, calculated for conditions expected at CFHT, Hawaii: $r_0 = 30$ cm, $\tau = 0.1$, SNR $= 5$ for target $K = 5$ (see Baudoz et al. [4,12]). Center: numerical simulation (based on a phase error map of HST) of residual energy profile for observation in K window (2.2 μm; $\Delta\lambda = 0.4$ μm), and expressed in magnitude differences. Right: behaviour of SNR versus ΔK the magnitude difference between star and companion; curves pertain to star K magnitudes 8 and 14. Dashed lines: optical quality is assumed the same as on HST, pointing instabilities eliminated. Solid lines: pointing residuals of 5 marcsec rms causes less than 3 magnitudes degradation. K window, quantum efficiency $\eta = 0.5$, $R = T = 0.5$, $S = 50$ m^2, optical transmission $t_{\text{opt}} = 0.1$, observing time 1000, ron $= 20e$/pix.

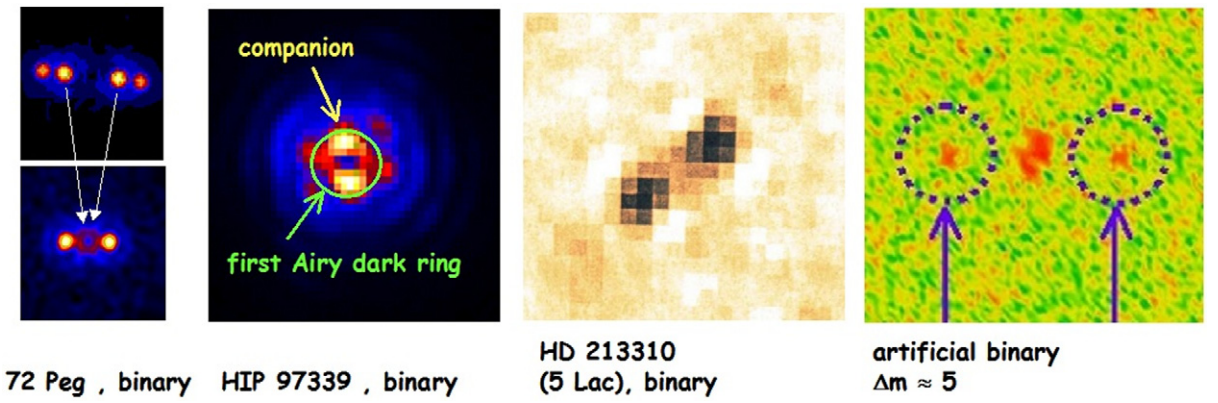

Fig. 10. Left, center left, center right: celestial sources, $\lambda = 2.2$ μm, $\Delta\lambda = 0.4$ μm. Left: disappearance when going on-axis, of bright component in binary 72 Peg, $K = 1.76$, $\Delta K = 0.36$, separation $\rho = 0.53$ arcsec, Airy ring $= 0.35$ arcsec, telescope 1.52 m OHP + Adaptive Optics, automatic intensity scale in image. Center left: example of close-sensing, companion of spectro binary HIP 97339, separation $\rho = 0.13$ arcsec, ΔK unknown (but modest), telescope 3.6 m CFH Hawaii + PUEO Adaptive Optics, Airy ring $= 0.15$ arcsec, exposure/frame $= 15$, 20 frames. $K = 3.5 \pm 0.5$, Airy ring $= 0.35$ arcsec, telescope 1.52 m OHP + Adaptive Optics. Poor seeing: average ($r_0 \approx 5$ cm), τ_0 unknown. Center right: binary HD 213310 (5 Lac), separation $\rho = 0.11$ arcsec (Airy/3), estimated $\Delta K = 3.5 \pm 0.5$, Airy ring $= 0.35$ arcsec, telescope 1.52 m OHP + Adaptive Optics. Poor seeing: average ($r_0 \approx 5$ cm). Right: laboratory artificial binary, separation roughly 2 Airy, conservative $\Delta K \cong 6$ (flux ratio larger than 300) with 512 frames, $\lambda = 2.2$ μm, bandwidth [1.9 μm; 2.6 μm] from laboratory class commercially available IR camera (Jade SWIR). Twin-images of companion appearing as little patches against noisy background.

5. Conclusions

In this article we have presented the main and specific features of our Achromatic Interfero Coronagraph (principle, theoretical capabilities and some results from test runs in the laboratory and behind a telescope). The main advantages of the AIC are the large spectral bandwidth over which the coronagraphic rejection is achievable and the very small Inner Working Angle (providing the capability to explore the very close angular neighbourhood of a source at a level better than that set by the diffraction-limit). The main drawback is the difficulty to achieve and to maintain equality of the optical paths at the required accuracy. Recently, an improved version of the device (regarding OPD fine-tuning) has been built and is presently under test. The next step is to accommodate this new AIC on a large telescope equipped with Adaptive Optics, so as to undertake scientific programs. New configurations, easier to accommodate in a telescope's optical train, are currently under study.

References

[1] J. Gay, Y. Rabbia, C. R. Acad. Sci. Paris Sér. IIb 322 (1996) 265–271.
[2] J. Gay, et al., C. R. Acad. Sci. Paris Sér. IIb 325 (1997) 51–56.
[3] P. Baudoz, PhD thesis, University of Nice–Sophia Antipolis, France, 1999.
[4] P. Baudoz, et al., Astron. Astrophys. Suppl. 141 (2000) 319–329.
[5] J. Gay, et al., in: EAS Publications "Astronomy with High Contrast Imaging", Nice, France, May 2002, 2003, pp. 245–257.
[6] Y. Rabbia, et al., in: Proc. ESO Workshop Science Drivers Future VLT/VLTI, 2001, pp. 273–278.
[7] C. Racine, et al., Publ. Astron. Soc. Pacific 111 (1999) 587.
[8] B. Lyot, C. R. Acad. Sci. Paris Ser. IIb 325 (1930) 51.
[9] D. Mouillet, Astron. Astrophys. 324 (1997) 1083.
[10] J.L. Beuzit, et al., Astron. Astrophys. Supl. 125 (1997) 175–182.
[11] J.P. Rivet, et al., in: Proc. of IAU Colloquium, Villefranche/Mer, France, October 2005, 2006, pp. 487–489.
[12] P. Baudoz, et al., Astron. Astrophys. Suppl. 145 (2000) 341–350.
[13] Y. Rabbia, et al., in: Proc. NGST Colloq., Liege, Belgium, ESA-SP 429, 1998, pp. 279–284.
[14] Y. Rabbia, et al., Proc. Colloquium INSU, Antarctic Dome C, Toulouse, juin 2004 (CD Rom).
[15] R.N. Bracewell, Nature 274 (1978) 780.
[16] C. Roddier, F. Roddier, Publ. Astron. Soc. Pacific 109 (1997) 815.
[17] D. Rouan, et al., Publ. Astron. Soc. Pacific 112 (777) (2000) 1479–1486.
[18] L. Abe, et al., Astron. Astrophys. 374 (2001) 1161–1168.
[19] O. Guyon, et al., Astron. J. Suppl. 167 (1) (2006) 81–99.
[20] J. Gay, et al., C. R. Physique 6 (2005) 1169–1175.
[21] J. Gay, et al., in: Proc. of IAU Colloquium, C 200, Villefranche/Mer, France, October 2005, 2006, pp. 473–477.
[22] C. Gouy, C. R. Acad. Sci. Paris 110 (1890) 1251.
[23] M. Born, E. Wolf, Principle of Optics, Pergamon Press, 1970.
[24] R.W. Boyd, J. Opt. Soc. Amer. 70 (1980) 877.
[25] J.W. Goodman, Introduction to Fourier Optics, McGraw–Hill, 1968.
[26] R. Bracewell, Fourier Transform and its Applications, McGraw–Hill, 1965.
[27] R.J. Noll, J. Opt. Soc. Amer. 66 (1976) 207.
[28] J.M. Conan, Ph.D. thesis, Université Paris XI Orsay, France, 1994.
[29] C. Verinaud, M. Carbillet, EAS Publications "Astronomy with High Contrast Imaging", Nice, France, May 2002, 2003, pp. 209–219.